

Spontaneous magnetization and anomalous Hall effect in an emergent Dice lattice

O. Dutta^{1,*}, A. Przysiężna^{1,2,3}, and J. Zakrzewski^{1,4}

¹ *Instytut Fizyki imienia Mariana Smoluchowskiego, Uniwersytet Jagielloński,
ulica Łojasiewicza 11, PL-30-348 Kraków, Poland*

² *Institute of Theoretical Physics and Astrophysics, University of Gdańsk, Wita Stwosza 57,
80-952 Gdańsk, Poland*

³ *National Quantum Information Centre of Gdańsk, Andersa 27, 81-824 Sopot, Poland*

⁴ *Mark Kac Complex Systems Research Center, Uniwersytet Jagielloński, Kraków, Poland*

(Dated: June 26, 2021)

Abstract

Ultracold atoms in optical lattices serve as a tool to model different physical phenomena appearing originally in condensed matter. To study magnetic phenomena one needs to engineer synthetic fields as atoms are neutral. Appropriately shaped optical potentials force atoms to mimic charged particles moving in a given field. We present the realization of artificial gauge fields for the observation of anomalous Hall effect. Two species of attractively interacting ultracold fermions are considered to be trapped in a shaken two dimensional triangular lattice. A combination of interaction induced tunneling and shaking can result in an emergent Dice lattice. In such a lattice the staggered synthetic magnetic flux appears and it can be controlled with external parameters. The obtained synthetic fields are non-Abelian. Depending on the tuning of the staggered flux we can obtain either anomalous Hall effect or its quantized version. Our results are reminiscent of Anomalous Hall conductivity in spin-orbit coupled ferromagnets.

PACS numbers: 67.85.Lm, 03.75.Lm, 73.43.-f

* E-mail: omjyoti@gmail.com

INTRODUCTION

Due to its unusual features such as quantized conductance and dissipation-less edge states, the Quantum Hall effect (QHE) [1] has various possible applications in quantum information sciences. In practical implementation, the standard QHE needs strong external magnetic fields and high mobility samples to occur. Therefore, it is particularly desirable to realize Hall effects without external magnetic fields.

In 1881, Hall [2] observed that in ferromagnetic materials there are unusually large Hall currents at low fields when compared to non-magnetic conductors [3]. Since then, theoretical explanation of this effect was a subject of a debate and it has taken a century until the physics of the phenomena were explained. This effect, known now as the anomalous Hall effect (AHE), originates from spontaneous magnetization in spin-orbit coupled ferromagnets [4–6]. The magnetization breaks the time reversal symmetry while the spin-orbit coupling induces nontrivial topology of the bands [7, 8]. It is not quantized for a metal, giving AHE, and quantized for insulators when Fermi energy lies in the band-gap, giving quantum anomalous Hall effect (QAHE). AHE and its quantized version can occur even in zero magnetic fields and they have been observed in various systems [5, 9–12].

Haldane [13] in 1988 gave a theoretical proposal of an AHE without spin orbit coupling. He presented a quantized Hall effect without Landau levels in a system with circulating currents on a honeycomb lattice where the time reversal symmetry is broken only locally. Since then concentrated effort have been put forward to simulate AHE without the presence of a magnetic field. The key point of such proposals is to engineer nontrivial topology of energy bands where the Hall conductance is related to the integral of the Berry curvature of the filled part of the band. To tune the band structure in order to change its topology and induce the anomalous Hall effect, we need to create non-Abelian synthetic gauge fields [14–18]. In the case of Ferromagnets it is done by spin-orbit coupling, in Haldane model – by circulating currents. In all of those proposals regarding AHE without magnetic field, one important ingredient is the presence of strong next-nearest neighbor tunneling with certain complex amplitude. Such a tunneling is in general hard to realize in normal lattices due to the exponential suppression of tunneling amplitudes with the distance. This presents another pertinent question: is it possible to generate AHE in a lattice with only the nearest neighbor tunneling? In the present paper we present such a lattice model leading to AHE

in the quantum regime.

We show that in two-dimensional lattice combined effect of interaction induced tunneling and shaking can induce AHE and QAHE (used in 1D, this ingredients can also lead to topological phenomena [19]). We focus on the systems of ultracold gases that provide versatile platform to simulate and engineer novel forms of matter [14]. Our proposal consists of attractive two-species fermions (as in [20]) trapped in a periodically shaken triangular lattice. Triangular lattice introduces geometrical frustration while the shaking can resonantly enhance the interaction-induced sp -orbital nearest neighbor tunneling. In effect, an emergent Dice lattice is formed accompanied by a strong staggered flux which, due to inclusion of p -orbitals, leads to a formation of synthetic non-Abelian fields. The system shows spontaneous magnetization accompanied by appearance of anomalous Hall conductivity forming an ultracold gas analogue of spin-orbit coupled ferromagnetic insulators. Furthermore, we show that, in presence of a strong staggered field, one can reach the regime of quantized Hall conductivity. This is a proposal of an experimentally realizable system with AHE without spin-orbit coupling.

RESULTS

The model

Consider an unequal mixture of two-species attractive ultracold fermions (denoted by \uparrow, \downarrow) trapped in a triangular lattice with fillings $n^\uparrow = 1/3$ and $n^\downarrow > 1/3$. A strong attractive contact interaction between atoms leads to pairing – formation of composites between the \uparrow and \downarrow -fermions, as studied experimentally for different lattice geometries [21–23]. We define a composite creation operator $\hat{c}_i^\dagger = \hat{s}_{i\uparrow}^\dagger \hat{s}_{i\downarrow}^\dagger$ with the corresponding number operator $\hat{n}_i^c = \hat{c}_i^\dagger \hat{c}_i$. $\hat{s}_{\sigma i}^\dagger, \hat{s}_{\sigma i}$ are the creation and annihilation operators of the σ fermions in the respective s -bands. The composites are hardcore bosons which anti-commute at the same site, $\{\hat{c}_i, \hat{c}_i^\dagger\} = 1$, and commute for different sites, $[\hat{c}_i, \hat{c}_j^\dagger] = 0$ for $\mathbf{i} \neq \mathbf{j}$ [24].

We consider three lowest bands of the triangular two-dimensional (2D) lattice (we assume some tight trap in the third direction as in typical 2D cold atoms experiments [25, 26]). For sufficiently deep optical lattices the structure of the bands may be understood using a harmonic approximation for separate sites. The lowest band is the s -band with two close in

energy p -orbitals forming the excited bands. Typically fermions (for low filling) reside in the s -band. However, once the composite occupies a given site an additional fermion coming to this site must land in the excited band due to the Pauli exclusion principle.

The harmonic approximation typically underestimates the tunneling coefficients (for a discussion see a recent review [28]). This is of no importance for the following since we assume that by using the well developed lattice shaking techniques, one can tune the standard intra-band tunneling to negligible values [25, 26, 29]. Such a shaking simultaneously makes the intra-band interaction induced tunneling [27, 30–34] (called also bond-charge tunneling) vanishingly small. The only remaining tunneling mechanism is then the sp -inter-band interaction induced tunneling [20] which can be resonantly enhanced adjusting the shaking frequency (note that the standard single-body tunneling between sp orbitals vanishes in Wannier function representation). Therefore, the system at low-energies consists of the composites and the excess \downarrow -fermions with filling $n^\downarrow - n^\uparrow$. Note that the \downarrow - or \uparrow -fermions of the composites cannot undergo sp -tunneling without breaking the strong pairing - which costs energy. Similarly, as discussed in detail in [22, 24], the tunneling of the composites to a neighboring vacant site as a whole is extremely small, (see Methods section) so it is neglected. Thus, the low-energy local Hilbert subspace is spanned by $\hat{c}_i^\dagger|0\rangle, \hat{p}_{\pm,i}^\dagger\hat{c}_i^\dagger|0\rangle$, and $\hat{s}_i^\dagger|0\rangle$ states, where $\hat{s}_i, \hat{p}_{\pm,i}$ denote the excess \downarrow -fermions operators in the s - and p -orbitals. The latter are written in the chiral representation $\hat{p}_\pm = (\hat{p}_x \pm i\hat{p}_y)/\sqrt{2}$. Within this subspace, one can show that the composite number operator equals the \uparrow -fermions number operator, $\hat{n}_i^c = \hat{n}_i^\uparrow$ and the densities $n^c = n^\uparrow = 1/3$. Other important relations are: i) $\hat{s}_i^\dagger\hat{c}_i^\dagger = 0$ - a composite and an excess s -fermion cannot occupy the same site due to the Pauli-exclusion principle; ii) $[\hat{n}_i^c, \hat{p}_{\pm,j}] = 0$, and iii) $[\hat{n}_i^c, \hat{s}_j] = 0$ for $\mathbf{i} \neq \mathbf{j}$.

The effective Hamiltonian for the composites and the excess \downarrow -fermions consists of three parts (see Methods for more details and Fig. 4 for visualization of tunnelings): H_{sp} describing interaction-induced sp -tunneling, H_{onsite} describing energies and local contact interactions, and $H_{shaking}$ describing the driving force. First of them reads,

$$\frac{H_{sp}}{J_{sp}} = \frac{1}{\sqrt{2}} \sum_{\mathbf{i}, \delta, \sigma = \pm} f_{\delta\sigma} \hat{p}_{\sigma,\mathbf{i}}^\dagger \hat{n}_i^c \hat{s}_{\mathbf{i}+\delta} + h.c., \quad (1)$$

where vectors connecting nearest-neighbors in the triangle lattice are $\boldsymbol{\delta} = \pm\boldsymbol{\delta}_0, \pm\boldsymbol{\delta}_\pm$ with $\boldsymbol{\delta}_0 = (1, 0), \boldsymbol{\delta}_+ = (1/2, \sqrt{3}/2), \boldsymbol{\delta}_- = (1/2, -\sqrt{3}/2)$. Due to the angles created by the different $\boldsymbol{\delta}$ vectors, in the chiral representation an additional phase factor f_δ appears. In the

harmonic approximation of the triangular lattice potential, this phase factor is given by $f_{\delta\sigma} = \exp[-i\sigma \tan^{-1}(\delta_y/\delta_x)]$. The tunneling J_{sp} is given in terms of the s - and p -band Wannier functions $W_{\mathbf{i}}^{00}(x, y)$ and $W_{\mathbf{i}}^{10}(x, y)$ as

$$J_{sp} = g_{2D} \int \int W_{\mathbf{i}}^{10}(x, y)(W_{\mathbf{i}}^{00}(x, y))^2 W_{\mathbf{i}+\delta_0}^{00}(x, y) dx dy, \quad (2)$$

with the contact interaction strength g_{2D} adjusted for a quasi-2D geometry (with a tight harmonic confinement along z) [35]. The second part gives the on-site Hamiltonian including higher band energy contribution and contact interactions. It reads [20],

$$H_{\text{onsite}} = U_2 \sum_{\mathbf{i}} \hat{n}_i^c + U_{sp} \sum_{\mathbf{i}, \sigma=\pm} \hat{n}_i^c \hat{n}_{\sigma\mathbf{i}} + E_1 \sum_{\mathbf{i}, \sigma=\pm} \hat{n}_{\sigma\mathbf{i}}, \quad (3)$$

where U_2 denotes the energy of the composites and U_{sp} is the additional interaction energy to occupy the p -orbital of a composite filled site. E_1 is the single-particle excitation energy of the p -band. Shaking with elliptical periodic driving force leads to [25],

$$H_{\text{shaking}} = \sum_{\mathbf{i}} \mathbf{i} \cdot \mathbf{F}_t (\hat{n}_{s\mathbf{i}} + \hat{n}_{+\mathbf{i}} + \hat{n}_{-\mathbf{i}}), \quad (4)$$

with the shaking force $\mathbf{F}_t = [-K_1 \sin(\Omega t)\hat{x} + K_2 \cos(\Omega t + \Phi)\hat{y}]$. We consider the case where $J_{sp} \ll U_2, U_{sp} \leq \Omega$. That allows us to use rotating-wave approximation and Floquet theorem and to average terms fast oscillating in time (see Methods).

The sp -tunneling will be resonantly enhanced when the energy to occupy the p -bands is an integer multiple of the shaking frequency. This translates into the condition that $E_1 + U_{sp} = N\Omega$ for integer N . The resonance order, N , can be controlled by varying either the lattice depth, interaction strength or the driving frequency. The time-averaged Hamiltonian then becomes,

$$\frac{H_{\text{avg}}}{J_{sp}} = \frac{1}{\sqrt{2}} \sum_{\mathbf{i}, \delta, \sigma=\pm} F_{\delta} f_{\delta\sigma} \hat{p}_{\sigma\mathbf{i}}^{\dagger} \hat{n}_i^c \hat{s}_{\mathbf{i}+\delta}, \quad (5)$$

where

$$F_{\delta} = \frac{1}{2\pi} \int_0^{2\pi} \exp[iN\Omega t - iK_{\delta} \cos(t + \alpha_{\delta})] dt = \mathcal{J}_N(K_{\delta}/\Omega) \exp[-iN\alpha_{\delta}], \quad (6)$$

with $\mathcal{J}_N(x)$ being the Bessel function of the first kind with integer order N . The amplitudes are $K_{\delta_0} = K_1$ and $K_{\delta_{\pm}} = [K_1^2 + 3K_2^2 \pm 2\sqrt{3}K_1K_2 \sin \Phi]^{1/2}$. The phase factor $\alpha_{\delta} = 0$ for $\delta = \pm\delta_0$ and $\alpha_{\delta} = \tan^{-1} \left[\frac{\sqrt{3} \cos \Phi}{1 \pm \sqrt{3} \sin \Phi} \right]$ for $\delta = \pm\delta_{\pm}$. The effective tunneling strength may be characterized by $J'_{sp}(N, \delta) = J_{sp} \mathcal{J}_N(K_{\delta}/\Omega)$. Moreover, lattice shaking also induces phases to the sp -tunnelings (6) as illustrated in Fig.1(a) (see also Methods).

The ground state composite structure

The composite number operator \hat{n}_i^c commutes with the Hamiltonian (5), $[\hat{n}_i^c, \hat{H}_{\text{avg}}] = 0$. Therefore, we can characterize a site by the presence or the absence of a composite, i.e. $n_i^c = 1, 0$ which makes the Hamiltonian, (5), quadratic in operators *for a particular realization* of composite configuration. For a given composite configuration, we then diagonalize the quadratic Hamiltonian and fill up the energy levels depending on the excess \downarrow -fermions filling $n^\downarrow - n^\uparrow \leq 1/3$. We find the ground state composite structure by comparing the energies of different composite configurations using simulated annealing on 6×6 up to 20×12 lattices with periodic boundary conditions. For details about the parameters of simulated annealing, we refer to Ref. [20]. The resulting ground state self-organized structure of the composites resembles a Dice lattice and is shown in Fig. 1(a). Its basis consists of three sites denoted A, B and C. The A site consists of two orbitals p_+ and p_- whereas the site B and C have only s -orbitals. The basis vectors for the Dice lattice are given by $\mathbf{a}_1 = (3/2, \sqrt{3}/2)$ and $\mathbf{a}_2 = (3/2, -\sqrt{3}/2)$. For any deviation from the $1/3$ filling of the composites, the excess composites or vacancies will show up as impurities on top of the Dice lattice as long as the density of such impurities is small ($n_{\text{imp}} \ll 1/3$).

To understand the origin of the Dice structure, consider first a composite at some chosen site A. The energy is minimized when all the neighboring sites (forming hexagon with the site A in the center) are without composites. This facilitates the sp tunneling from a p orbital at site A to the neighboring sites. Any composite on these neighboring sites increases the energy by $J_{\text{sp}}F_{\text{avg},\delta}$. Thus, for a composite filling of $n^c = 1/3$, the delocalization area is maximized by filling the lattice with hexagons with a composite at their center.

Assuming the ground state configuration is fixed, the effective Hamiltonian for the excess fermions is quadratic and thus easily diagonalized to yield the band structure. The behavior of the excess fermions is then that of an ideal Fermi gas with such band structure, which is easily computed.

Creation of the staggered field

For the Dice lattice considered here, one can construct two kind of plaquettes: i) The three plaquettes as shown in Fig. 1(b) where the particle traverses the closed path involving

$p_x \leftrightarrow s \leftrightarrow p_x \leftrightarrow s$ orbitals. Such a path does not mix the p_x and p_y orbitals. Due to the phases of the tunneling amplitudes, a particle going through each of those plaquettes (denoted by φ_1, φ_2 and φ_3 , see Fig.1(b) and calculated along the direction of the arrow) acquire fluxes due to Aharonov-Bohm effect. We find that the induced flux is staggered in nature as the phases obey the constraint $\text{mod}(\varphi_1 + \varphi_2 + \varphi_3, 2\pi) = 0$. These fluxes are calculated by taking into account a single p-orbital. Fig. 1(c) shows the flux strengths for $N = 1$. In particular, for $\Phi = 0$, $\varphi_1 = \varphi_2 = \varphi_3 = 2\pi/3$ which is equivalent to a uniform magnetic flux of the same magnitude. With growing Φ , fluxes change with all fluxes vanishing at $\Phi = \pi/2$.

ii) The other kind of plaquette involves the A sites containing p_x, p_y orbitals as given by the parallelogram shown in Fig. 1(d). A particle going around such plaquette picks up a non-Abelian flux. Consider the transport from site “1” to “2”. The process can go either via the upper or the lower path with two consecutive sp tunnelings with strengths $J'_{\text{sp}}(N, \delta_0) = J_{\text{sp}} \mathcal{J}_N(K_{\delta_0}/\Omega)$ and $J'_{\text{sp}}(N, \delta_+) = J_{\text{sp}} \mathcal{J}_N(K_{\delta_+}/\Omega)$. The effective amplitude becomes $\mathcal{T}_{12} = J'_{\text{sp}}(N, \delta_0) J'_{\text{sp}}(N, \delta_+)/2$. The kinetic energy term around the plaquette for A sites may be written as

$$H_{\text{kin},A} = \Psi_2^\dagger \mathcal{T}_{12} L_{12} \Psi_1 + \Psi_3^\dagger \mathcal{T}_{23} L_{23} \Psi_2 + \Psi_4^\dagger \mathcal{T}_{34} L_{34} \Psi_3 + \Psi_1^\dagger \mathcal{T}_{41} L_{41} \Psi_4 + h.c., \quad (7)$$

where the array $\Psi_l = (p_+, p_-)_l$ denotes p -orbitals at site l . The corresponding link variables connecting the neighboring A sites along the clockwise direction are given by 2×2 matrix L_{mn} with

$$L_{12} = \begin{pmatrix} \cos(\pi/3 + \alpha_{\delta_+}) & e^{i\pi/3} \cos \alpha_{\delta_+} \\ e^{-i\pi/3} \cos \alpha_{\delta_+} & \cos(\pi/3 - \alpha_{\delta_+}) \end{pmatrix}. \quad (8)$$

L_{23} (\mathcal{T}_{23}) is given by changing $\pi/3 \rightarrow -\pi/3$ and $\delta_+ \rightarrow \delta_-$ in the expression for L_{12} (\mathcal{T}_{23}). Moreover, we find that $L_{12} = L_{34}$ and $L_{23} = L_{41}$ with similar relations for \mathcal{T}_{ij}) and they depend on the staggered flux through the phase of the tunneling amplitudes. The link variables are not unitary, which makes it not straightforward to describe them as synthetic non-Abelian fields. Nonetheless one can polar decompose them to, $L_{mn} = \mathcal{S}_{mn} \mathcal{U}_{mn}$, where $\mathcal{U}_{mn}^\dagger \mathcal{U}_{mn} = 1$. Such decompositions are possible as the L_{nm} matrices are positive semi-definite. Then one can define a corresponding Wilson loop parameter [36]

$$W = \text{Tr} [\mathcal{U}_{12} \mathcal{U}_{23} \mathcal{U}_{34} \mathcal{U}_{41}]. \quad (9)$$

The Wilson loop parameter has (i) an intrinsic contribution (appearing at $\Phi = \pi/2$, with no staggered flux through an individual plaquette in Fig. 1(b) due to the appearance of the sp -band tunneling and (ii) an extrinsic contribution due to the external staggered flux induced by shaking. As a result, the link matrices are of non-Abelian nature ($W \neq 2$) for any shaking phase Φ .

Spontaneous magnetization

First, we study the behavior of the system in the absence of staggered flux realized for $N = 1, \Phi = \pi/2$ Fig. (1). The effective non-Abelian field is intrinsic in nature and the corresponding dispersion relation for the lowest energy band is shown in Fig. 2a. The main characteristic of the dispersion relation is the appearance of two non-equivalent Dirac cones and disappearance of flat bands. This is in contrast to the dispersion relation in a normal Dice lattice where the dispersion relation contains an intersecting Dirac cone and a flat band. Moreover, above a certain Fermi energy (of the excess fermions), the first two bands are degenerate. When we introduce the staggered flux, the dispersion changes and the gap opens at the band touching points (Fig. 2b). Once the Fermi energy is higher than the gap, the two bands become degenerate again. This is in a stark contrast to other situations with nearest neighbor tunneling where staggered flux leads only to the movement of the Dirac cones [37, 38] and to opening a gap one either needs long-distance tunneling [13, 17], uniform magnetic field or synthetic non-Abelian fields along with magnetic field [39].

Anomalous Hall effect

Consider the local magnetization (\mathcal{M}_z) in position space as well as magnetization in momentum space defined as

$$\begin{aligned}\mathcal{M}_z &= \langle \hat{n}_{\mathbf{i}+} \rangle - \langle \hat{n}_{\mathbf{i}-} \rangle, \\ \mathcal{M}_{\mathbf{k}} &= \langle \hat{n}_{\mathbf{k}+} \rangle - \langle \hat{n}_{\mathbf{k}-} \rangle.\end{aligned}\tag{10}$$

A non-zero local magnetization characterizes the breaking of time-reversal symmetry as the particles acquire local angular momentum due to the particle number difference between the p_+ and p_- orbitals. First, we find that the presence of non-zero staggered flux immediately

results in non-zero \mathcal{M}_z and in opening of the gap. Thus, appearance of non-zero \mathcal{M}_z can be used as an indirect evidence for the presence of a gap in our system. The local magnetization is shown in Fig.2c (dashed line) for a small staggered flux. It vanishes only when the first two bands are totally filled. The presence of spontaneous magnetization (spontaneous time-reversal symmetry breaking) is reminiscent of spin-orbit coupled ferromagnets [4]. Moreover, to look into the topological nature of the system, we define the intrinsic Hall conductivity,

$$\sigma_{xy} = \sum_{\epsilon_n < \epsilon_F} \Omega_n(\mathbf{k})/2\pi. \quad (11)$$

The Berry curvature, $\Omega_n(\mathbf{k})$, for the n -th band is given by $\Omega_n(\mathbf{k}) = \nabla_{\mathbf{k}} \times \langle u_{n\mathbf{q}} | \nabla_{\mathbf{k}} | u_{n\mathbf{q}} \rangle$ where $|u_{n\mathbf{q}}\rangle$ denotes an eigenvector for the n -th band. The total Hall conductivity σ_{xy} then depends on the Fermi energy ϵ_F of the system as shown in [Fig.2c (solid line)]. We find that the local Berry curvature is concentrated near the Dirac points which results in a non-zero contribution to σ_{xy}^n when ϵ_F is in the band. As ϵ_F enters the band gap, we find that σ_{xy}^n flattens at a value $> 1/2$. This can be ascribed to the presence of two Dirac cones near the band gap. As we increase ϵ_F , the contribution from the next band begins to play a role and eventually the conductivity changes sign. The second peak appears when the Fermi energy reaches the maximum of the first band. Such structures in conductivity have been predicted to arise due to the presence of magnetic monopoles in the momentum space [40].

Quantum Anomalous Hall effect

Finally, consider the strong flux limit, e.g the case of $\Phi = 0$ where the flux through each plaquette is $2\pi/3$. Strong flux results in lifting the degeneracy between the first two bands (Fig. 3, top plot). The middle two bands still touch each other in the form of Dirac cones. With the degeneracy lifted, one can define Chern numbers given by $\nu = (2, -4, 2)$ resulting in the appearance of Quantum Anomalous Hall effect. We have also calculated the Hall conductivity and when the Fermi energy of the excess fermions resides in the band gap, conductivity becomes integer valued (Fig. 3, bottom plot). The magnitude of the band gap is $\approx J_{sp}$. For a triangular lattice (lattice constant $a = 500\text{nm}$) with lattice depth of $6E_R$ and transverse frequency of $10E_R$, the sp tunneling strength in the harmonic approximation is given by $J_{sp} \sim 0.008E_R$ assuming the scattering length of -400 Bohr radius. This corresponds to a band gap of about ~ 10 nano-Kelvin which determines the temperature

regime where the Hall phase can be observed. For the Dice lattice with dilute impurities, the Hall conductivity presented in this paper remain unchanged due to the topological nature of the Berry curvature for the dispersion bands [4]. The band topology discussed here can be measured in principle by using recently proposed methods of Ramsey interferometry and Bloch oscillations [41, 42], or from momentum distribution from Time-of-Flight images [43]. Moreover, the generation of local orbital angular momentum due to broken time-reversal symmetry in the chiral p -orbitals can also be detected by time-of-flight measurements [44].

CONCLUSIONS

To summarize, we considered an unequal mixture of attractively interacting fermions in a shaken triangular lattice. Pairing produces immobile composites that gives rise to Dice lattice for the excess fermions. Adjustments of shaking frequency and amplitude allow to make intra-band tunnelings negligible while resonantly enhancing interaction-induced sp -tunnelings for the excess fermions. Moreover, shaking leads to the controlled staggered magnetic field and induces (on the p -orbitals) non-Abelian character of the system. Their joint effect leads to spontaneous chiral magnetization (due to time reversal symmetry breaking) along with appearance of Anomalous Hall effect. Many fascinating question related to the findings here can be investigated further including the role of impurities, long-range interaction etc. Moreover, by using dipolar atoms, one can further study many-body effects like superconductivity [45, 46], density-waves in presence of the artificial non-Abelian gauge fields presented here.

ACKNOWLEDGMENTS

We thank M. Lewenstein and K. Sacha for enlightening discussions. This work was realized under National Science Center (Poland) project No. DEC-2012/04/A/ST2/00088. A.P. is supported by the International PhD Project "Physics of future quantum-based information technologies", grant MPD/2009-3/4 from Foundation for Polish Science and by the University of Gdansk grant BW 538-5400-B169-13-1E.

AUTHOR CONTRIBUTIONS

O.D., A.P., J.Z. conceived the idea, performed derivations and calculations, discussed the results and wrote the manuscript.

ADDITIONAL INFORMATION

The authors declare no competing financial interests.

METHODS

The model Hamiltonian

We consider an unequal mixture of two-species ultracold fermions (denoted by \uparrow, \downarrow) assuming strong attractive interactions between two species. It is then energetically favorable for fermions to pair, the low energy system is then effectively composed of paired composites and the excess \downarrow fermions. We denote the creation and annihilation operators for \uparrow fermions as $\hat{s}_{\uparrow\mathbf{i}}^\dagger$ and $\hat{s}_{\uparrow\mathbf{i}}$. For the more abundant \downarrow fermions we include both s and p orbitals denoting the corresponding operators as $\hat{s}_{\downarrow\mathbf{i}}^\dagger, \hat{s}_{\downarrow\mathbf{i}}, \hat{p}_{\downarrow\pm\mathbf{i}}^\dagger, \hat{p}_{\downarrow\pm\mathbf{i}}$. In the main text, for simplicity, we have neglected \uparrow -fermion tunneling and all the intra-band tunnelings for \downarrow -fermions from the beginning. Here, let us derive the Hamiltonian without these assumptions and show that, indeed, these effects may be neglected.

The full time-dependent Hamiltonian $H(t)$ consists of three parts $H(t) = H_{\text{tun}} + H_{\text{onsite}} + H_{\text{shaking}}$. The first, H_{tun} describes the tunnelings, H_{onsite} describes the on-site interactions and H_{shaking} describes the shaking. Together they read:

$$\begin{aligned}
 H_{\text{tun}} &= J_0 \sum_{\mathbf{i}, \delta} \hat{s}_{\uparrow\mathbf{i}}^\dagger \hat{s}_{\uparrow\mathbf{i}+\delta} + J_0 \sum_{\mathbf{i}, \delta} \hat{s}_{\downarrow\mathbf{i}}^\dagger \hat{s}_{\downarrow\mathbf{i}+\delta} \\
 &+ \sum_{\mathbf{i}, \delta, \sigma} J_1^{\sigma\delta} \hat{p}_{\downarrow\sigma, \mathbf{i}}^\dagger \hat{p}_{\downarrow\sigma, \mathbf{i}+\delta} + \sum_{\mathbf{i}, \delta, \sigma} J_{11}^{\sigma\delta} \hat{p}_{\downarrow\sigma, \mathbf{i}}^\dagger (\hat{n}_{\mathbf{i}}^\uparrow + \hat{n}_{\mathbf{i}+\delta}^\uparrow) \hat{p}_{\downarrow\sigma, \mathbf{i}+\delta} \\
 &+ \frac{J_{sp}}{\sqrt{2}} \sum_{\mathbf{i}, \delta, \sigma=\pm} \left(f_\delta \hat{p}_{\downarrow\sigma, \mathbf{i}}^\dagger \hat{n}_{\mathbf{i}}^\uparrow \hat{s}_{\downarrow\mathbf{i}+\delta} + h.c. \right), \tag{12} \\
 H_{\text{onsite}} &= U_2 \sum_{\mathbf{i}} \hat{n}_{\mathbf{i}}^\uparrow \hat{n}_{\mathbf{si}}^\downarrow + U_{01} \sum_{\mathbf{i}, \sigma=\pm} \hat{n}_{\sigma\mathbf{i}}^\downarrow \hat{n}_{\mathbf{i}}^\uparrow + E_1 \sum_{\mathbf{i}, \sigma=\pm} \hat{n}_{\sigma\mathbf{i}}^\downarrow, \\
 H_{\text{shaking}} &= \sum_{\mathbf{i}} \mathbf{i} \cdot \mathbf{F}_t (\hat{n}_{\mathbf{si}}^\downarrow + \hat{n}_{+\mathbf{i}}^\downarrow + \hat{n}_{-\mathbf{i}}^\downarrow + \hat{n}_{\mathbf{si}}^\uparrow).
 \end{aligned}$$

Here, $\hat{n}_i^{\uparrow(\downarrow)}$, denote number operators of \uparrow (\downarrow) fermions respectively while $\hat{n}_{\pm}^{\downarrow}$ are number operators for the \downarrow p -fermions with \pm -chirality. The same amplitude, J_0 corresponds to the standard tunneling between s orbitals, the corresponding tunneling in the p -band is described by $J_1^{\sigma\delta}$. Moreover, we include density induced (bond-charge) intra-band tunneling for p -orbitals with strength $J_{11}^{\sigma\delta}$. J_{sp} is the amplitude of the hopping between s and p bands which is also induced by the interaction with \uparrow fermions. The various tunneling processes in Hamiltonian (12) are shown in Fig. 4. The tunneling amplitudes are given by

$$\begin{aligned}
J_0 &= \int \int \mathcal{W}_i^{00}(x, y) H_{\text{latt}} \mathcal{W}_{i+\delta}^{00}(x, y) dx dy \\
J_1^{\sigma\delta} &= \int \int [\mathcal{W}_i^{\sigma}(x, y)]^* H_{\text{latt}} \mathcal{W}_{i+\delta}^{\sigma}(x, y) dx dy \\
J_{11}^{\sigma\delta} &= g_{2D} \int \int [\mathcal{W}_i^{\sigma}(x, y)]^* [\mathcal{W}_i^{00}(x, y)]^2 \mathcal{W}_{i+\delta}^{\sigma}(x, y) dx dy,
\end{aligned} \tag{13}$$

where $\mathcal{W}_i^{00}(x, y)$ is the Wannier function of the s -band and $\mathcal{W}_i^{\sigma}(x, y)$ with $\sigma = \pm$ are the Wannier functions corresponding to p_+ -and p_- -bands in the harmonic approximation for the triangular lattice potential. The single particle Hamiltonian for the triangular lattice is denoted by H_{latt} .

Note that the Hamiltonian (12) does not contain tunnelings of the composites themselves. Such a pair tunneling term can arise due to interaction [28] but is 3-4 orders of magnitude smaller than other tunneling terms. The composites can also tunnel via higher-order processes (discussed in [22]). The leading term of this collective tunneling is of the second order [24] with the corresponding amplitude being proportional to $J_0^2/|U_2|$, i.e. very small assuming strong attraction. The effect is further reduced by assumed shaking - modification of effective J_0 - so such tunnelings can be safely neglected.

Low-energy and resonant subspaces

Now we define the low-energy subspace and the resonant subspace which are coupled by the driving (shaking). First we assume the strong interaction limit i.e. $J_0, J_1^{\sigma\delta}, J_{11}^{\sigma\delta}, J_{sp} \ll U_2, U_{01}$. Yet larger energy scale is set by single particle energy of the p band E_1 and the shaking frequency. Thus we assume $U_2, U_{sp} \ll E_1 \sim \Omega$. $|U_2|$ - the strength of attraction between \uparrow and \downarrow fermions sets the low-energy scale, thus we restrict the analysis to the subspace of Hilbert space where all \uparrow minority fermions are paired with their \downarrow partners. Thus

the low-energy local subspace is spanned by $\hat{s}_{\downarrow\mathbf{i}}^\dagger\hat{s}_{\uparrow\mathbf{i}}^\dagger|0\rangle, \hat{s}_{\downarrow\mathbf{i}}^\dagger|0\rangle$ states. As we will show below, due to the sp tunneling and periodic driving this subspace is resonantly connected to the subspace where a paired site can be occupied by p -orbital fermions, $\hat{p}_{\downarrow\sigma,\mathbf{i}}^\dagger\hat{s}_{\downarrow\mathbf{i}}^\dagger\hat{s}_{\uparrow\mathbf{i}}^\dagger|0\rangle$ with energy $E_1 + U_{01}$. Therefore, from now on our Hilbert space will consist of $\hat{s}_{\downarrow\mathbf{i}}^\dagger\hat{s}_{\uparrow\mathbf{i}}^\dagger|0\rangle, \hat{s}_{\downarrow\mathbf{i}}^\dagger|0\rangle, \hat{p}_{\downarrow\sigma,\mathbf{i}}^\dagger\hat{s}_{\downarrow\mathbf{i}}^\dagger\hat{s}_{\uparrow\mathbf{i}}^\dagger|0\rangle$ states.

We now apply the unitary transformation, $\hat{U}_t = \exp[-iH_{\text{onsite}}t - i\int_0^t H_{\text{shaking}}(t')dt']$ transferring the time-dependence in the total Hamiltonian $H(t)$ into the tunneling amplitudes. The new Hamiltonian $H' = \hat{U}^\dagger H \hat{U} - i\hat{U}^\dagger[d_t\hat{U}]$ is given by

$$\begin{aligned}
H' = & J_0 \sum_{\mathbf{i},\delta} \exp[-iU_2(\hat{n}_{\mathbf{i}}^\downarrow - \hat{n}_{\mathbf{i}+\delta}^\downarrow)t - i\boldsymbol{\delta} \cdot \mathbf{W}_t] \hat{s}_{\uparrow\mathbf{i}}^\dagger \hat{s}_{\uparrow\mathbf{i}+\delta} \\
& + J_0 \sum_{\mathbf{i},\delta} \exp[-iU_2(\hat{n}_{\mathbf{i}}^\uparrow - \hat{n}_{\mathbf{i}+\delta}^\uparrow)t - i\boldsymbol{\delta} \cdot \mathbf{W}_t] \hat{s}_{\downarrow\mathbf{i}}^\dagger \hat{s}_{\downarrow\mathbf{i}+\delta} \\
& + \sum_{\mathbf{i},\delta,\sigma} \exp[-iU_{01}(\hat{n}_{\mathbf{i}}^\uparrow - \hat{n}_{\mathbf{i}+\delta}^\uparrow)t - i\boldsymbol{\delta} \cdot \mathbf{W}_t] \\
& \times \hat{p}_{\downarrow\sigma,\mathbf{i}}^\dagger \left[J_1^{\sigma\delta} + J_{11}^{\sigma\delta}(\hat{n}_{\mathbf{i}}^\uparrow + \hat{n}_{\mathbf{i}+\delta}^\uparrow) \right] \hat{p}_{\downarrow\sigma,\mathbf{i}+\delta} \\
& + \frac{J_{sp}}{\sqrt{2}} \sum_{\mathbf{i},\delta,\sigma=\pm} \exp[-iE_1t - iU_{01}t - i\boldsymbol{\delta} \cdot \mathbf{W}_t] f_\delta \hat{p}_{\downarrow\sigma,\mathbf{i}}^\dagger \hat{n}_{\mathbf{i}}^\uparrow \hat{s}_{\downarrow\mathbf{i}+\delta},
\end{aligned} \tag{14}$$

where $\mathbf{W}_t = \int_0^t \mathbf{F}_\nu dt'$. We expand the exponential functions in (14) as: $\exp[-i\boldsymbol{\delta} \cdot \mathbf{W}_t] = \sum_n \mathcal{J}_n(K_\delta/\Omega) \exp[-in\Omega t]$. Then as $U_2 \ll \Omega$, after rotating-wave approximation (RWA) and projecting on our local Hilbert space, the first term of Hamiltonian (14) may be resonant only if U_2 contribution vanishes. Since this term corresponds to \uparrow -fermion tunneling (which appear paired only in our subspace) this process is possible only if a paired state and a \downarrow -fermion in s -orbital are neighbors (Fig. 1(a)). Otherwise the pair (composite) is pinned. Similarly, the second term may be resonant ($n_{\mathbf{si}}^\uparrow = n_{\mathbf{si}+\delta}^\uparrow = 0$) when a \downarrow -fermion in s -orbital tunnels to a neighboring empty site. The third term gives a resonant contribution via the tunneling process depicted in Fig.4(b). After RWA, all the time-independent tunneling amplitudes of the above intra-band tunnelings are changed by a factor $\mathcal{J}_0(K_\delta/\Omega)$. We see that to minimize the ss and pp tunnelings we have to tune the shaking amplitude such that $\mathcal{J}_0(K_{\delta_0}/\Omega) = 0$ and $\mathcal{J}_0(K_{\delta_-}/\Omega) = 0$. This assures that for the shaking phase $\Phi = 0$, there is no intra-band tunneling along the $\boldsymbol{\delta}_+$ direction as $K_{\delta_+} = K_{\delta_-}$.

In the last term of Hamiltonian (14) the fast oscillation with $E_1 + U_{01}$ frequency must be compensated by appropriate Fourier component yielding the sp resonant condition $E_1 + U_{01} = N\Omega$. Inspecting the tunneling term we see that, the tunneling in p -band is resonantly enhanced only when the composite density in neighboring sites \mathbf{i} and $\mathbf{i} + \boldsymbol{\delta}$ follows the relation

$(n_{\mathbf{i}}^\uparrow - n_{\mathbf{i}+\boldsymbol{\delta}}^\uparrow) = 1$. Due to the type of sp coupling in Hamiltonian, (14), p -fermions may appear only in composite occupied sites. This may occur only from a site occupied by a lonely \downarrow -fermion (if there were a composite at that site, an additional energy difference, U_2 , the pair energy would appear bringing the system out of the chosen resonance). After carrying RWA and in the limit of vanishing intra-band tunneling, the effective Hamiltonian reads,

$$H' = \frac{J_{sp}}{\sqrt{2}} \sum_{\mathbf{i}, \boldsymbol{\delta}, \sigma = \pm} \mathcal{J}_N(K_{\boldsymbol{\delta}}/\Omega) \exp[-i\sigma \tan^{-1}(\delta_y/\delta_x)] \hat{p}_{\downarrow, \sigma, \mathbf{i}}^\dagger \hat{n}_{\mathbf{i}}^\uparrow \hat{s}_{\downarrow, \mathbf{i}+\boldsymbol{\delta}}, \quad (15)$$

where $\mathcal{J}_N(x)$ defines Bessel function of order- N . We see that, one can control the different tunneling amplitudes by tuning the shaking amplitude, frequency and interaction strength.

When the shaking phase $\Phi \neq 0$, along $\boldsymbol{\delta}_0$ and $\boldsymbol{\delta}_-$ directions the intra-band tunneling still vanishes, but remains nonzero along $\boldsymbol{\delta}_+$ direction. Amplitude of the latter can be tuned to values smaller than the sp -tunneling amplitude by changing the interaction strength. Moreover, once the Dice structure of the composites is created, the only possible tunneling along $\boldsymbol{\delta}_+$ direction is the inter-band sp tunneling (compare Fig.1(a) in the main text). So, adding small intra-band tunneling due to a finite shaking phase will not destabilize the Dice structure.

Effects of tunneling on the emergent lattice

In this section, we discuss the effect of the tunneling on the Dice lattice structure. As discussed before, a composite can tunnel to a vacant site only via higher order processes [22, 24] which are negligible for large $|U_2|$. So the only way a composite can tunnel is if the minority fermion tunnels to a site already occupied by a majority fermion in s -orbital site as shown in the first figure in Fig.4. Such a process can be described by an effective tunneling for the composite coupled to the tunneling of the excess fermions in the opposite direction. To investigate the effect of such a tunneling we use a one-dimensional minimal model,

$$H_{\min} = -\frac{J_{sp}}{\sqrt{2}} \sum_{\langle ij \rangle} \left[\hat{p}_i^\dagger \hat{n}_i^c \hat{s}_j + h.c \right] - J_0 \sum_{\langle ij \rangle} \left[\hat{c}_i^\dagger \hat{c}_j \hat{s}_j^\dagger \hat{s}_i \right], \quad (16)$$

where at each site i we have only s - and p -orbitals, and $\langle ij \rangle$ denotes the nearest neighbors. We have introduced operators $\hat{c}_i, \hat{c}_i^\dagger$ as the composite annihilation and creation operators. The first term denotes the composite density dependent sp tunneling of the excess fermions and the last term just denotes the composite tunneling and excess fermion tunneling. When

$J_0 = 0$, the ground state is given by the composite structure, $n_{2i}^c = 1, n_{2i+1}^c = 0$ when composite filling is $n^c = 1/2$. Such a density wave structure is equivalent to the Dice lattice structure we study in a triangular lattice. Due to the hardcore bosonic nature of the composites, we use a factorized variational composite wavefunction, $|\Phi_c\rangle = \prod_i |\Phi_c\rangle_i$, where $|\Phi_c\rangle_{2i} = \cos\theta|1\rangle_c + \sin\theta|0\rangle_c$ and $|\Phi_c\rangle_{2i+1} = \cos\theta|0\rangle_c + \sin\theta|1\rangle_c$ and $|1\rangle_c, |0\rangle_c$ denote a composite occupied or empty site. In the composite wavefunction ansatz, θ is the variational parameter. The density wave state at $J_0 = 0$ is obtained for $\theta = 0$. Using such an ansatz, we can integrate over the composite subspace and get an effective Hamiltonian,

$$H_{\text{eff}} = \frac{J_{\text{sp}} \cos^2 \theta}{\sqrt{2}} \sum_{\langle i \rangle} \left[\hat{p}_{2i}^\dagger \hat{s}_{2i+1} + h.c. \right] + \frac{J_{\text{sp}} \sin^2 \theta}{\sqrt{2}} \sum_{\langle i \rangle} \left[\hat{p}_{2i+1}^\dagger \hat{s}_{2i} + h.c. \right] - J_0 \frac{\sin^2 2\theta}{4} \sum_{\langle ij \rangle} \hat{s}_i^\dagger \hat{s}_j. \quad (17)$$

Then we write the energy for excess fermion filling $n = 1/4$ (this is $1/2$ of the previous value due to the doubling of number of degrees of freedom) for $\theta \ll 1$ and $J_{\text{sp}} \gg J_0$ as $E_{\text{var}} = \frac{2\sqrt{2}J_{\text{sp}}}{\pi} [-1 + \theta^2] + O(\theta^4)$, which is independent of composite tunneling. From that we conclude that the energy is minimized for $\theta = 0$. For larger tunneling strength J_0 , we have compared the energy of the homogenous state with $\theta = \pi/4$ and the density wave state with $\theta = 0$ finding that the density wave state has lower energy as long as $J_{\text{sp}} > 3J_0/4$. Though the present calculation is one-dimensional, the essential physics also applies to the more complicated situation of triangular lattice, where we expect the Dice lattice density wave structure to be stable even in the presence of small composite tunneling.

-
- [1] Klitzing K., Dorda G., and Pepper M., New Method for High-Accuracy Determination of the Fine-Structure Constant Based on Quantized Hall Resistance, *Phys. Rev. Lett.* **45** 494 (1980).
 - [2] Hall E., On the ‘‘Rotational Coefficient’’ in nickel and cobalt *Phil. Mag.* **12**, 157 (1881).
 - [3] Hall E., On a New Action of the Magnet on Electric Currents *Am. J. Math.* **2**, 287 (1879).
 - [4] Nagaosa N., Sinova J., Onoda S., MacDonald A. H., and Ong N. P., Anomalous Hall effect, *Rev. Mod. Phys.* **82**, 1539 (2010).
 - [5] Yu R., *et. al.*, Quantized anomalous Hall effect in magnetic topological insulators, *Science* **329**, 61 (2010).

- [6] Chang C.-Z., *et. al.*, Experimental Observation of the Quantum Anomalous Hall Effect in a Magnetic Topological Insulator, *Science* **340**, 167 (2013).
- [7] Hasan M. Z. and Kane C. L., Colloquium: Topological insulator, *Rev. Mod. Phys.* **82**, 3045 (2010).
- [8] Qi X. L., and Zhang S. C., Topological insulators and superconductors, *Rev. Mod. Phys.* **83**, 1057 (2011).
- [9] Qi X. L., Wu Y. S., and Zhang S. C., Topological quantization of the spin Hall effect in two-dimensional paramagnetic semiconductors, *Phys. Rev. B* **74**, 085308 (2006).
- [10] Qi X. L., Hughes T. L. , and Zhang S. C., Topological field theory of time-reversal invariant insulators, *Phys. Rev. B* **78**, 195424 (2008).
- [11] Liu C. X., Qi X. L., Dai X., Fang Z., and Zhang S. C., Quantum Anomalous Hall Effect in $\text{Hg}_{1-y}\text{Mn}_y\text{Te}$ Quantum Wells, *Phys. Rev. Lett.* **101**, 146802 (2008).
- [12] Nomura K., and Nagaosa N., Surface-Quantized Anomalous Hall Current and the Magnetoelectric Effect in Magnetically Disordered Topological Insulators, *Phys. Rev. Lett.* **106**, 166802 (2011).
- [13] Haldane F. D. M., Model for a Quantum Hall Effect without Landau Levels: Condensed-Matter Realization of the “Parity Anomaly”, *Phys. Rev. Lett.* **61**, 2015 (1988).
- [14] Lewenstein M., Sanpera A., and Ahufinger V., Ultracold Atoms in Optical Lattices: Simulating quantum many-body systems, *Oxford University Press*, London, (2012).
- [15] Terças H., Flayac H., Solnyshkov D. D., and Malpuech G., Non-Abelian Gauge Fields in Photonic Cavities and Photonic Superfluids, *Phys. Rev. Lett.* **112**, 066402 (2014)
- [16] Lin Y.-J. , Jiménez-García K. , and Spielman I. B., A spin-orbit coupled Bose-Einstein condensate, *Nature* **471**, 83-86 (2011).
- [17] P. Hauke, *et. al.*, Non-Abelian Gauge Fields and Topological Insulators in Shaken Optical Lattices, *Phys. Rev. Lett.* **109**, 145301 (2012).
- [18] Kosior A., and Sacha K., Simulation of non-Abelian lattice gauge fields with a single component gas, *Euro. Phys. Lett.* **107**, 26006 (2014).
- [19] Przysiężna A., Dutta O., and Zakrzewski J., Rice-Mele model with topological solitons in an optical lattice, *New J. Phys.* **17**, 013018 (2015).
- [20] Dutta O., Przysiężna A., and Lewenstein M., Emergent non-trivial lattices for topological insulators, *Phys. Rev. A* **89**, 043602 (2014).

- [21] Chin J. K., *et. al.*, Evidence for superfluidity of ultracold fermions in an optical lattice, *Nature* **443**, 961 (2006).
- [22] Strohmaier N. *et. al.*, Interaction-Controlled Transport of an Ultracold Fermi Gas, *Phys. Rev. Lett.* **99**, 220601 (2007).
- [23] Hackermüller L. *et. al.*, Anomalous expansion of attractively interacting fermionic atoms in an optical lattice, *Science* **327**, 1621 (2010).
- [24] Micnas R., Ranninger J., and Robaszkiewicz S., Superconductivity in narrow-band systems with local nonretarded attractive interactions, *Rev. Mod. Phys.* **62**, 113 (1990).
- [25] Struck J., *et. al.*, Quantum Simulation of Frustrated Classical Magnetism in Triangular Optical Lattices, *Science* **333**, 996 (2011).
- [26] Struck J., *et. al.*, Engineering Ising-XY spin-models in a triangular lattice using tunable artificial gauge fields, *Nat. Phys.* **9**, 738 (2013).
- [27] Hirsch J. E., Bond-charge repulsion and hole superconductivity, *Physica C* **158**, 326 (1989).
- [28] Dutta O., *et. al.*, Non-standard Hubbard models in optical lattices: a review arXiv:1406.0181
- [29] Eckardt A., Weiss C., and Holthaus M., Superfluid-Insulator Transition in a Periodically Driven Optical Lattice, *Phys. Rev. Lett.* **95**, 260404 (2005),
- [30] Best T. S., *et. al.*, Role of Interactions in ^{87}Rb - ^{40}K Bose-Fermi Mixtures in a 3D Optical Lattice *Phys. Rev. Lett.* **102**, 030408 (2009).
- [31] Dutta O., Eckardt A., Hauke P., Malomed B., and Lewenstein M., Bose-Hubbard model with occupation-dependent parameters *New. J. Phys.* **12**, 023019 (2011).
- [32] Mering A. and Fleischhauer M., Multiband and nonlinear hopping corrections to the three-dimensional Bose-Fermi-Hubbard model *Phys. Rev. A* **83**, 063630 (2011).
- [33] Lühmann D.-S., Jürgensen O., and Sengstock K., Multi-orbital and density-induced tunneling of bosons in optical lattices, *New. J. Phys.* **14**, 033021 (2012).
- [34] Łącki M., Delande F., and Zakrzewski J., Dynamics of cold bosons in optical lattices: effects of higher Bloch bands *New. J. Phys.* **15**, 013062 (2013).
- [35] Petrov D. S., Holzmann M., and Shlyapnikov G. V., Bose-Einstein Condensation in Quasi-2D Trapped Gases *Phys. Rev. Lett.* **84**, 2551 (2000).
- [36] C. Wetterich, Linear lattice gauge theory, Arxiv: 1307.0722 (2013).
- [37] L. Tarruell, *et. al.*, Creating, moving and merging Dirac points with a Fermi gas in a tunable honeycomb lattice, *Nature* **483**, 302 (2012).

- [38] Lim L.-K., Hemmerich A., and Smith C. M., Artificial staggered magnetic field for ultracold atoms in optical lattices *Phys. Rev. A* **81**, 023404 (2010).
- [39] Goldman N., *et. al.*, Non-Abelian Optical Lattices: Anomalous Quantum Hall Effect and Dirac Fermions *Phys. Rev. Lett.* **103**, 035301 (2009).
- [40] Fang Z., *et. al.*, The Anomalous Hall Effect and Magnetic Monopoles in Momentum Space *Science* **302**, 92 (2003).
- [41] Abanin D. A., Kitagawa T., Bloch I., and Demler E., Interferometric Approach to Measuring Band Topology in 2D Optical Lattices, *Phys. Rev. Lett.* **110**, 165304 (2013).
- [42] Atala M., *et. al.*, Direct measurement of the Zak phase in topological Bloch bands *Nat. Phys.* **9**, 795 (2013).
- [43] Dong-Ling D., Shengtao W., and Duan L. -M., Arxiv: 1407.1146 (2014).
- [44] Wirth G., Ölschläger M., and Hemmerich A., Evidence for orbital superfluidity in the P-band of a bipartite optical square lattice *Nat. Phys.* **7**, 147 (2011).
- [45] Lim L. -K., Lazarides A., Hemmerich A., and Smith C. M., Strongly interacting two-dimensional Dirac fermions *Euro. Phys. Lett.* **88**, 36001 (2009).
- [46] Kubasiak A., Massignan P., and Lewenstein M., Topological superfluids on a lattice with non-Abelian gauge fields *Euro. Phys. Lett.* **92** 46004 (2010).

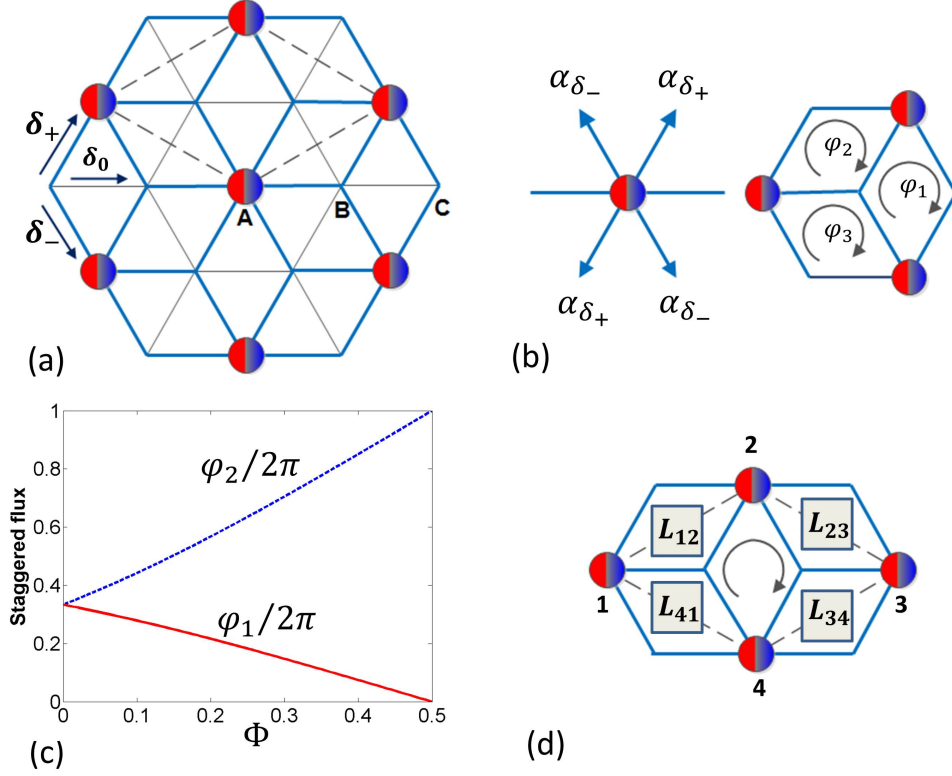


FIG. 1. (a) The representation of the system considered in the paper. Red-and-blue spheres refer to the composites. The thin lines denote the bonds in the original triangular lattice and the blue lines represent the bonds for the excess \downarrow -fermions in the emerged dice lattice. On the composite occupied sites we have p -orbitals for the excess fermions while on vacant sites we have s -orbitals for the excess fermions. δ_0, δ_{\pm} correspond to the vectors connecting the nearest neighbors and the sites **A, B, C** symbolize the basis for the Dice lattice. (b) Left panel: The tunneling phases described in Eq.(6). Right panel: Three elementary cells present in the dice lattice and the corresponding fluxes in those cells. The arrows show the direction along which the fluxes are calculated. (c) The magnitude of the fluxes in each cell plotted as a function of the shaking phase Φ (in the units of π). (d) The elementary plaquette for the A sites in the dice lattice along with the matrices L_{l+1} coupling the sites l and $l + 1$.

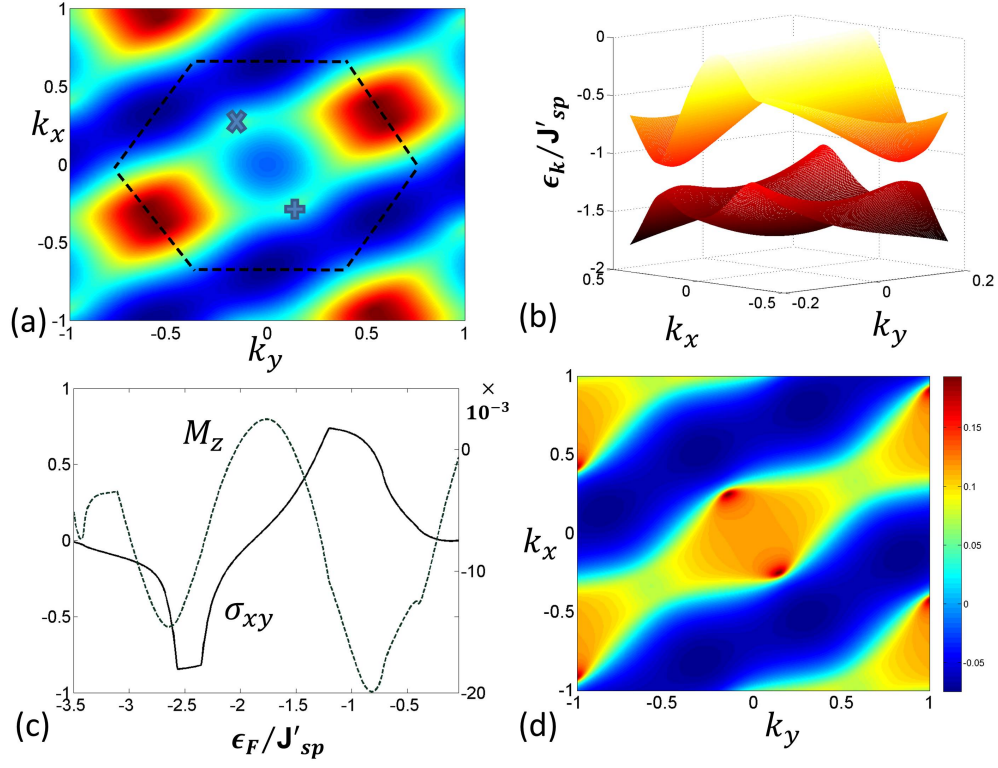


FIG. 2. (a) The dispersion relation for the lowest energy band as a function of a lattice momentum \mathbf{k} for zero staggered flux, $\varphi_1 = \varphi_2 = \varphi_3 = 0$ corresponding to shaking phase $\Phi = \pi/2$ and $N = 1$. The dark blue part denotes low energy regions. The \times and $+$ denote positions of Dirac points. (b) The dispersion $\epsilon_{\mathbf{k}}$ for the first two band in the presence of small staggered flux for $\Phi = \pi/4$. The presence of the staggered flux along with the non-Abelian nature of the system helps to open a gap near the Dirac points. The tunneling strength is given by $J'_{sp} = J_{sp}J_1(K_1/\Omega)$. (c) The magnetization (10) and Hall conductivity as a function of Fermi energy for $\Phi = \pi/4$ and $N = 1$. Spontaneous magnetization appears due to time-reversal symmetry breaking. The Berry curvature has a non-zero contribution near the band-touching points. Contribution of local Berry curvature from such band-touching points results in a finite Hall conductivity which shows plateau like structure due to the presence of the gap between the first two bands. (d) The magnetization $\mathcal{M}_{\mathbf{k}}$ in momentum space (from Eq. (10)) as a function of crystal momentum \mathbf{k} shows sharp peaks near the two Dirac points for $\Phi = \pi/4$ and $N = 1$. They correspond to the presence of monopole like structure in the corresponding Berry phase.

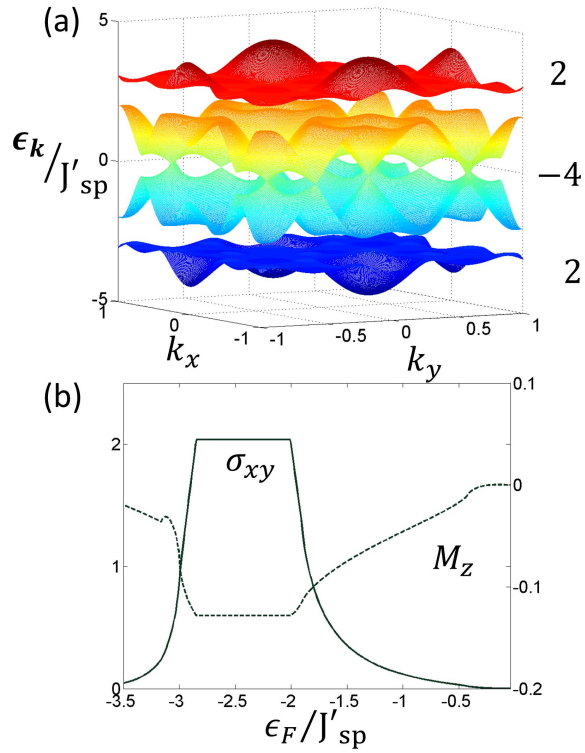


FIG. 3. (a) The dispersion relation for $\Phi = 0$ which corresponds to staggered flux with $\varphi_1 = \varphi_2 = 2\pi/3$ and $N = 1$. The numbers on the right hand side of the figure show the invariant Chern numbers corresponding to the respective bands. As we have seen in Fig.2(a), there are multiple Dirac cones which touch each other in the zero flux limit. Thus, when there is a band gap, there are contributions to Berry curvature coming from all such points. This gives rise to bands with large Chern numbers $(2, -4, 2)$. Plot (b) represents the Hall conductivity σ_{xy} and the magnetization \mathcal{M}_z for that case.

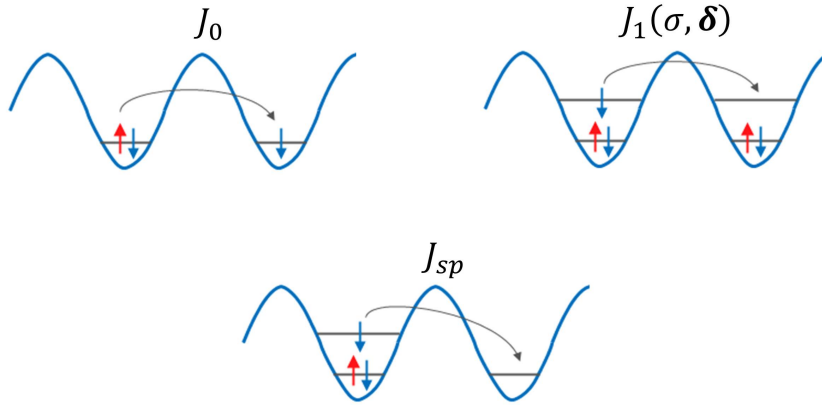


FIG. 4. Pictorial representation of different tunneling processes in Hamiltonian, Eq.(12). The top left panel describes the resonant tunneling process where a \uparrow fermion from a composite tunnel to a neighboring excess \downarrow -fermion occupied site. This tunneling process corresponds to the first term in Hamiltonian H_{tun} . The top right panel describes the process when an excess fermion can tunnel in the p -band resonantly provided both the sites are already occupied by composites. This reflects the third term in Hamiltonian H_{tun} . The bottom figure depicts the interaction induced sp tunneling amplitude.